Critical temperature oscillations in magnetically coupled superconducting mesoscopic loops

M. Morelle,[1] V. Bruyndoncx,[1] R. Jonckheere,[2] and V. V. Moshchalkov[1]
[1]*Laboratorium voor Vaste-Stoffysica en Magnetisme, K.U. Leuven, Celestijnenlaan 200D, B-3001 Leuven, Belgium*
[2]*Interuniversity Micro-Electronics Center, Kapeldreef 75, B-3001 Leuven, Belgium*
(Received 27 April 2000; revised manuscript received 30 January 2001; published 23 July 2001)

We study the magnetic interaction between two superconducting concentric mesoscopic Al loops, close to the superconducting/normal phase transition. The phase boundary is measured resistively for the two-loop structure as well as for a reference single loop. In both systems Little-Parks oscillations, periodic in field, are observed in the critical temperature T_c versus applied magnetic field H. In the Fourier spectrum of the $T_c(H)$ oscillations, a weak ''low frequency'' response shows up, which can be attributed to the inner loop supercurrent magnetic coupling to the flux of the outer loop. The amplitude of this effect can be tuned by varying the applied transport current.

DOI: 10.1103/PhysRevB.64.064516 PACS number(s): 74.25.Dw, 74.60.Ec, 73.23.−b

I. INTRODUCTION

In 1962, Little and Parks[1] measured a mesoscopic superconducting cylinder in an axial magnetic field. The superconducting critical temperature $T_c(\Phi/\Phi_0)$ showed oscillations periodic in the normalized flux, with the period corresponding to the superconducting flux quantum $\Phi_0=h/2e$. These oscillations in $T_c(\Phi/\Phi_0)$ are a straightforward consequence of the fluxoid quantization constraint, which was introduced by London.[2] Fluxoid quantization can be easily understood by integrating the second Ginzburg-Landau (GL) equation for the supercurrent[3,4]

$$\vec{j}=\frac{2e}{m^*}|\Psi|^2(\hbar\vec{\nabla}\delta-2e\vec{A})=2e|\Psi|^2\vec{v} \tag{1}$$

along a closed contour. Here, $\vec{j}$ is the supercurrent density, $\vec{v}$ is the superfluid velocity, δ is the phase of the complex order parameter $\Psi=|\Psi|e^{i\delta}$, and $\vec{A}$ is the magnetic vector potential. Integration along an arbitrary closed contour yields the following equation:

$$\Phi'\equiv\Phi+\frac{1}{2e}\oint m^*\vec{v}\cdot d\vec{l}=N\Phi_0, \tag{2}$$

where the fluxoid Φ' is quantized in units of $\Phi_0=h/2e$ and Φ is the applied flux threading the area inside the contour. The integer number N is the phase winding number, or also called the fluxoid quantum number, counting the number of flux quanta Φ_0 penetrating the enclosed area. When the applied flux Φ is not equal to integer times the flux quantum Φ_0, a supercurrent j has to be generated in order to fulfill Eq. (2).

For a superconducting ring of radius r, made of wires of vanishing width ($w=0$), a one-dimensional (1D) GL model can be used to describe the onset of superconductivity. The relative T_c variations can be written as

$$\frac{T_{c0}-T_c(\Phi/\Phi_0)}{T_{c0}}=\frac{\xi^2(0)}{r^2}\left(N-\frac{\Phi}{\Phi_0}\right)^2, \tag{3}$$

where $\xi(0)$ is the coherence length at zero temperature, T_{c0} is the critical temperature in zero field , and the integer number N is chosen to maximize the critical temperature $T_c(\Phi)$. For each fluxoid quantum number N, the critical temperature $T_c(\Phi/\Phi_0)$ has a parabolic shape. The Little-Parks (LP) oscillations appear due to the transitions from the integer value N to $N+1$, at a half integer value of Φ/Φ_0. For $\Phi/\Phi_0=N$, no supercurrent flows in the ring, while for $\Phi/\Phi_0=N+1/2$, the supercurrent reaches a maximal value and changes sign. The maximum normalized variation of the critical temperature $\Delta T_c(\Phi/\Phi_0)/T_{c0}$ is $\xi^2(0)/4r^2$, as can be evaluated from Eq. (3). To observe these quantization effects experimentally, structures with the radius of the loop of the order of the coherence length $\xi(0)$ should be used.

Since the pioneering work of Little and Parks, single mesoscopic superconducting loops and cylinders has been largely studied. Recently, Zhu *et al.*[5] studied the flux state in two magnetically coupled mesoscopic normal loops. The magnetic coupling of an array of normal[6] and superconducting[7] loops has also been studied. In those cases the loops are electrically isolated from each other and can only interact magnetically.

Our work will focus on *the magnetic coupling of two concentric superconducting loops.* The modification of the phase boundary $T_c(H)$ of the outer loop due to magnetic coupling with the inner loop will be studied. Magnetic coupling effects between two loops are potentially very important since for the two loops made from different materials, a new unusual effect of enhancing $T_{c1}(H)$ due to a higher $T_{c2}(H)$ can be expected.

The GL free energy for such a system can be written as follows:

$$\mathcal{F}_s=\mathcal{F}_n+V_i\left(\alpha|\Psi_i|^2+\beta|\Psi_i|^4+\frac{m^*v_i^2}{2}|\Psi_i|^2\right)+V_o\left(\alpha|\Psi_o|^2+\beta|\Psi_o|^4+\frac{m^*v_o^2}{2}|\Psi_o|^2\right)+L_iI_i^2+L_oI_o^2+MI_iI_o, \tag{4}$$

with $\mathcal{F}_n$ the total free energy in the normal state, α and β the expansion coefficients, m^* the mass of a Cooper pair and L and M the self- and mutual inductance. V is the volume of

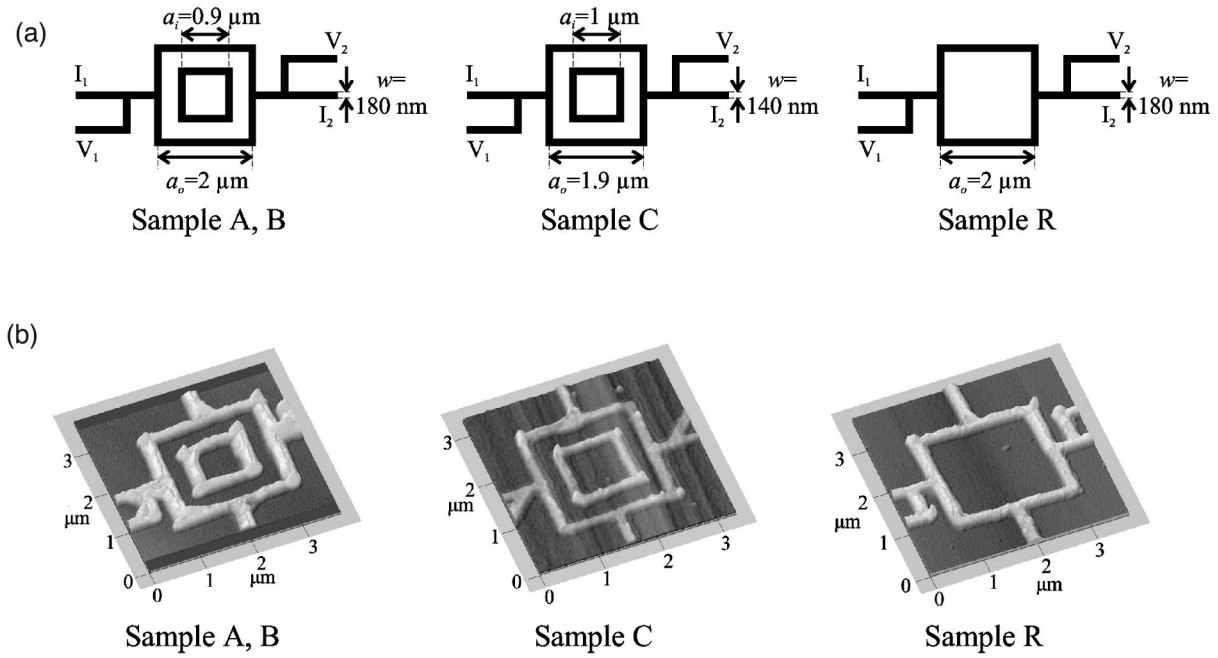

FIG. 1. (a) A schematic drawing of samples A, B, and C, and sample R. I_1 and I_2 are the contacts for the transport current; V_1 and V_2 are the voltage probes. a_i and a_o are the width of the inner, respectively outer loop, measured from middle to middle, and w is the wire width of the loop and of the connecting wires. (b) AFM image of the double loop (samples A, B, and C) and of the single loop (sample R).

the loop, Ψ is the order parameter, v is the velocity of the superfluid and I is the supercurrent. The indexes i and o refer to the inner and outer loop, respectively. The superfluid velocities of the two loops are determined from the fluxoid quantization constraint:

$$v_i = \frac{\hbar}{m^* r_i}\left(N_i - \frac{\Phi + I_o M}{\Phi_0}\right),$$

$$v_o = \frac{\hbar}{m^* r_o}\left(N_o - \frac{\Phi + I_i M}{\Phi_0}\right). \tag{5}$$

To solve this equation, the free energy must be minimized with respect to variations in Ψ_i, Ψ_o, I_i and I_o. The free energy $\mathcal{F}_s$ contains in this case the term $MI_iI_o \propto M|\Psi_i|^2|\Psi_o|^2$ responsible for the mixing of the two individual order parameters Ψ_i and Ψ_o.

II. EXPERIMENTAL RESULTS AND DISCUSSION

We present the results of transport measurements carried out on two different types of mesoscopic Al structures (Fig. 1). The first type of sample is composed of two concentric loops, with the outer loop being electrically connected to the experimental setup in order to perform four-points resistance measurements. Three samples of this type have been studied: sample A and sample B with the same thickness and the same dimensions of the loops and sample C with a smaller thickness and slightly different dimensions of the loops. The reference sample (sample R) is analogous to the first structure, but without the inner loop. All the samples discussed, except sample C, are evaporated in the same run. All samples have been prepared by thermal evaporation of 99.9999% pure Al on a SiO_2 substrate. The patterns are defined using electron beam lithography on a bilayer of *PMMA/PMMA-coPMMA* resist before the deposition of an aluminum film with a thickness $\tau = 50$ nm and $\tau = 28$ nm for samples A, B, and R and for sample C, respectively. After the evaporation, the liftoff was performed using dichloromethane. In Fig. 1(a), the geometry and the dimensions of the different structures are shown. The thickness and the lateral dimensions of the samples have been characterized by the x-ray diffraction on a coevaporated plane film and AFM [see Fig. 1(b)], respectively. The wire width of the loop and of the connecting wires has been determined from SEM investigations. The superconducting/normal phase boundaries are obtained from transport measurements, carried out with a transport current I_t flowing through the outer loop. The phase boundary is measured holding the resistance at a fixed resistive criterion (we used the criterion $R_n/2$, with R_n the resistance in the normal state). This is achieved using an electronic feedback circuit. Once a required temperature stability is obtained, the magnetic field is swept at a very slow rate (with a typical frequency of 20 μHz). To improve the signal-to-noise ratio a PAR 124A lock-in amplifier has been used, operating at 27.7 Hz.

The width of the wires of the studied superconducting loops determines the parabolic background of the $T_c(H)$ phase boundary:[8]

$$\frac{T_{c0} - T_c(H)}{T_{c0}} = \frac{\pi^2}{3}\left(\frac{w\xi(0)\mu_0 H}{\Phi_0}\right)^2, \tag{6}$$

TABLE I. Material parameters for the measured samples.

Sample	R	A	B	C
τ (nm)	50	50	50	28
w (nm)	180	180	180	140
a_o (μm)	2	2	2	1.9
a_i (μm)		0.9	0.9	1
T_{c0} (K)	1.324	1.326	1.327	1.363
$R_\square$ (Ω)$=\rho/\tau$ (4.2 K)	0.65	0.72	0.76	1.36
$l_{\rm el}$ (nm)	12.3	11	10.6	10.5
$\xi(0)$ [Eq. (6)] (nm)	103	105	102	117
$\xi(0)$ Ref. sample (nm)	128	128	128	
$\xi(0)$ dirty limit (nm)	114	112	120	112
L_i (pH)		1.6	1.6	1.9
L_o (pH)	4.5	4.5	4.5	4.6
M (pH)		22	22	21

where w is the width of the wires. Equation (6) also describes the $T_c(H)$ line for a superconducting thin film of thickness w subjected to a magnetic field parallel to the film plane. In a practical situation, the phase boundary of a superconducting loop of finite wire width will show a parabolic background [see Eq. (6)]. The suppression of T_c can be written as the sum of two components: an oscillatory term as described by Eq. (3), and a monotonic term [Eq. (6)]. The coherence length $\xi(0)$ of the samples can be determined from the parabolic background of the phase boundary, since the width of the wires w is a known parameter. A second method to evaluate the coherence length is to determine $\xi(0)$ from the slope of $T_c(H)$ of a coevaporated macroscopic reference film. A third method is based on the dirty limit of the GL theory,[3] where from the known value of the elastic mean free path l, the coherence length $\xi(0)=0.86\sqrt{\xi_0 l}$ is obtained, using the clean limit value $\xi_0=1.6$ μm for Al. The results of the three methods are summarized in Table I. The difference between the $\xi(0)$ values calculated with the three different methods can be partially explained by the rather broad error margins on the wire width w.

In Fig. 2, the theoretical phase boundaries are shown for the two single loops when they are not coupled magnetically: one using the dimensions of the inner loop to calculate the phase boundary (solid line), and the other using the size of the outer loop (lowest dashed line), thus corresponding to the reference sample; this has been calculated from Eq. (3) using the dimensions of the loops summarized in Table I. It should be mentioned that an increase along the vertical axis corresponds to a decreasing temperature. The amplitude of the LP oscillations is the larger the smaller the loop size [see Eq. (3)]. The period of the $T_c(H)$ oscillations for the inner and outer loop is given by $\mu_0\Delta H_i=\Phi_0/S_i$, and $\mu_0\Delta H_o=\Phi_0/S_o$, respectively with $S_i=a_i^2$ and $S_o=a_o^2$ the enclosed areas (see Fig. 1). Points X and Y in Fig. 2 are situated at two fixed applied magnetic field values on the T-H phase boundary for the outer loop. In the case of point X, the inner loop is in the normal state, thus the inner loop carries no supercurrent. In this situation, no flux is coupled to the outer loop. For point Y, on the contrary, the inner loop is in the superconducting state, and a supercurrent will flow in both loops in order to satisfy the respective fluxoid quantization constraints [Eq. (2)]. Under these conditions, due to the mutual inductance between the two current loops [see Eqs. (4) and (5)], an influence of the fluxoid quantization in the inner loop on the measured $T_c(H)$ phase boundary of the outer loop is expected.

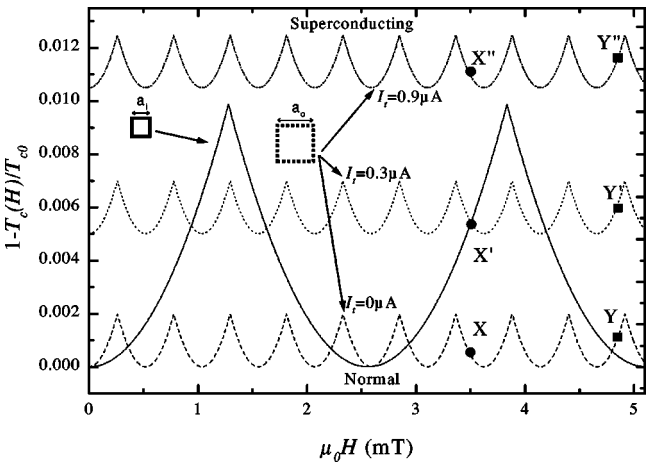

FIG. 2. Calculated phase boundary $T_c(H)$ of the inner (solid line) and outer loop (dashed, dotted, and dashed-dotted line) for two periods of the inner loop, without magnetic interaction, using the dimensions of samples A and B. The phase boundary of the outer loop is shown for three different transport currents I_t: $I_t=0$ μA dashed line, $I_t=0.3$ μA dotted line, and $I_t=0.9$ μA dashed-dotted line. The coherence length $\xi(0)=103$ nm is taken. The shift of the $T_c(H)$ curves with increasing I_t are estimated from Refs. 10 and 11: $I_c=I_{c0}(T_{c0}-T_c)^{3/2}$, with $I_{c0}\approx 550$ μA.

To extend the flux interval for which the inner loop remains superconducting, a higher transport current I_t can be applied to the outer loop. The phase boundary $T_c(\Phi)$ of the outer loop is schematically presented in Fig. 2 by the dotted ($I_t=0.3$ μA) and the dashed-dotted ($I_t=0.9$ μA) lines. We now follow through the fixed magnetic field lines following the points $X\rightarrow X''$ and $Y\rightarrow Y''$ by increasing the transport current I_t. The point on the phase boundary of the outer loop, with the same magnetic field value as X for $I_t=0$, will cross the phase boundary of the inner loop in point X' by increasing I_t. For a highest transport current, the inner loop will be superconducting for each point on the phase boundary of the outer loop (dashed-dotted line). The inner loop will be deeper in the superconducting state, following the shift from Y to Y'' while increasing the transport current. As a result, an increase of I_t will not only broaden the interval in which the inner loop is superconducting, but also increase the supercurrent in the inner loop.

Zhang *et al.*[9] have calculated the self-flux for a typical mesoscopic ring. From these calculations, we can find the self-flux and the additional flux in the outer loop due to the presence of the inner loop. The self-flux for the inner and outer loop will not be larger than 0.4% of the applied flux for $T/T_c>0.99$. The additional flux MI_i in the outer loop will be less than 4% in this temperature interval but can be higher than 20% for $T/T_c<0.95$. All the measurement presented in this paper are in the region $T/T_c>0.99$. A possibility to fur-

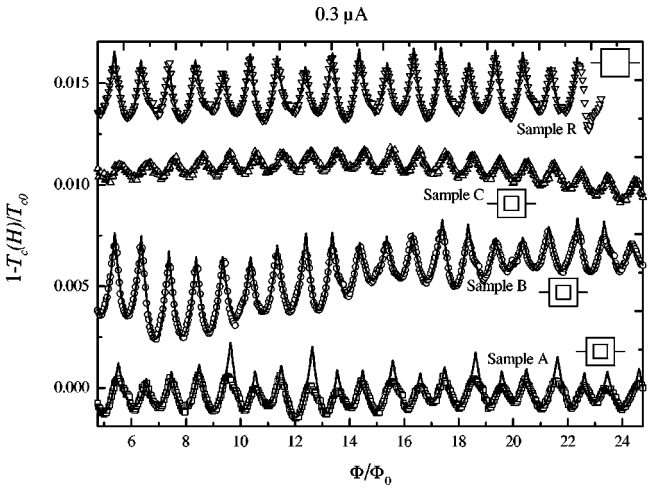

FIG. 3. Measured phase boundary $T_c(\Phi)$ after subtraction of the parabolic background caused by the finite wire width of the loops. The phase boundary is plotted in normalized units of the flux $\Phi = S_o \mu_0 H$ threading the outer loop. Within each oscillation period, a parabolic function is fitted through the data points in between the transition to a different fluxoid quantum number N_o. The phase boundary of sample A (□), sample B (○), sample C (△), and sample R (▽) is compared for the same transport current $I_t = 0.3$ μA.

ther increase the supercurrent in the inner loop I_i and thus the magnetic coupling between the two loops would be the use of a material with a higher T_c for the inner loop.

In Fig. 3, the phase boundaries of the samples A, B, C, and R (□: sample A; ○: sample B; △: sample C; ▽: sample R) are shown for a ac transport current $I_t = 0.3$ μA rms after subtraction of the monotonic parabolic background due to the finite width of the strips [Eq. (6)]. Further on, the flux $\Phi = S_o \mu_0 H$ will refer to the flux threading the surface of the outer loop. The $T_c(\Phi)$ part below 5 Φ_0 is not shown because the experimental data were rather noisy in the low field region for some measurements. The curves corresponding to different samples are arbitrarily shifted in Fig. 3. The variation of the critical temperature with increasing transport current can be estimated from Refs. 10 and 11 for zero field: $I_c = I_{c0}(T_{c0} - T_c)^{3/2}$, with $I_{c0} \approx 550$ μA and $I_{c0} \approx 240$ μA for samples A, B, and R and for sample C, respectively. The critical temperatures of the different samples after extrapolation of the experimental results to $I_t = 0$ are given in Table I. For $I_t = 0.3$ μA, the shift of the zero field critical temperature ΔT_{c0} (used in Fig. 2) is 7 mK (12 mK for sample C), for 0.5 μA: 9 mK and for 0.7 μA: 12 mK. Within each oscillation period, a parabolic function is fitted through the data points in between the transition to a different fluxoid quantum number $N_o \rightarrow N_o + 1$ [Eq. (3)]. The value for the self- and mutual inductance[12] for the different samples are summarized in Table I.

In Fig. 3, a smaller amplitude of the oscillations is observed for sample C, compared to the other samples. This smaller amplitude is to be expected because of a smaller thickness of the film, what would lead to a reduced mean free path and a smaller coherence length value for sample C

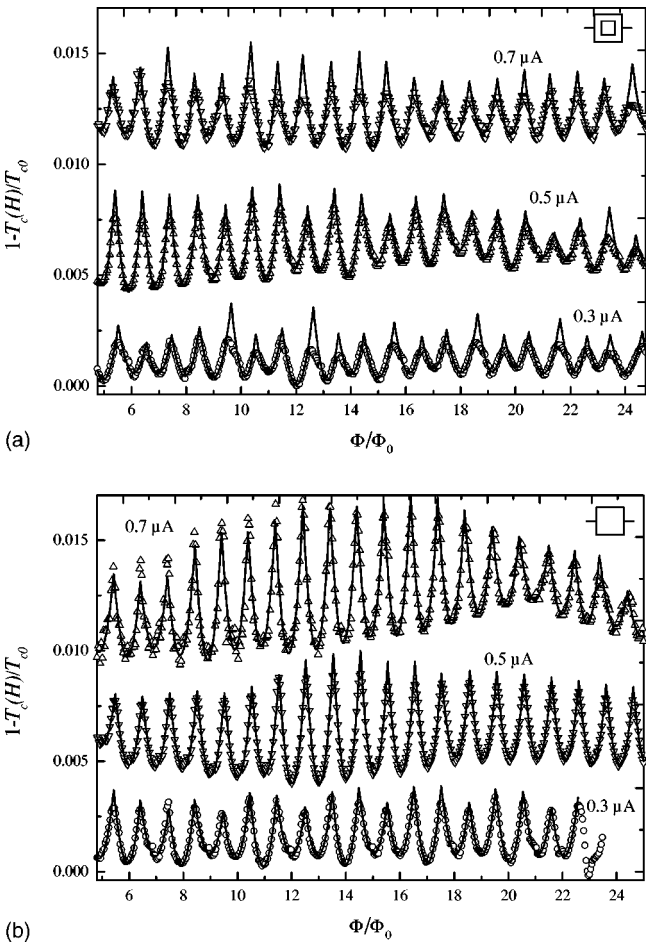

FIG. 4. Measured phase boundary $T_c(\Phi)$ after subtraction of the parabolic background caused by the finite wire width of the loops. The phase boundary is plotted in normalized units of the flux $\Phi = S_o \mu_0 H$ threading the outer loop. Within each oscillation period, a parabolic function is fitted through the data points in between the transition to a different fluxoid quantum number N_o. The results for three different ac transport currents I_t (○: 0.3 μA; △: 0.5 μA; ▽: 0.7 μA) are presented (a) for sample A and (b) for sample R.

[see Eq. (3)]. But the coherence lengths are comparable for all four different samples (see Table I).

The phase boundaries of the double loop sample A and for the reference sample R are also measured for different transport currents I_t. The results for three different ac transport currents I_t (○: 0.3 μA; △: 0.5 μA; ▽: 0.7 μA rms) are shown in Figs. 4(a) and 4(b) for sample A and sample R, respectively. From these experimental data, clear differences between sample A and sample R are seen. First of all, the amplitude of the $T_c(\Phi)$ oscillations is stronger in sample R, secondly the phase boundary of the single loop [Fig. 4(b)] matches very well with the fitted parabolic curves (solid curves), while the oscillations of sample A [Fig. 4(a)] are not parabolic at all, since the cusps in $T_c(\Phi)$ are always rounded.

The rounding of the cusps in $T_c(\Phi)$, observed for sample A, are not reproduced in samples B and C (see Fig. 3). These rounded cusps cannot be attributed with all certainty to the magnetic interactions with the inner loop, but may be also

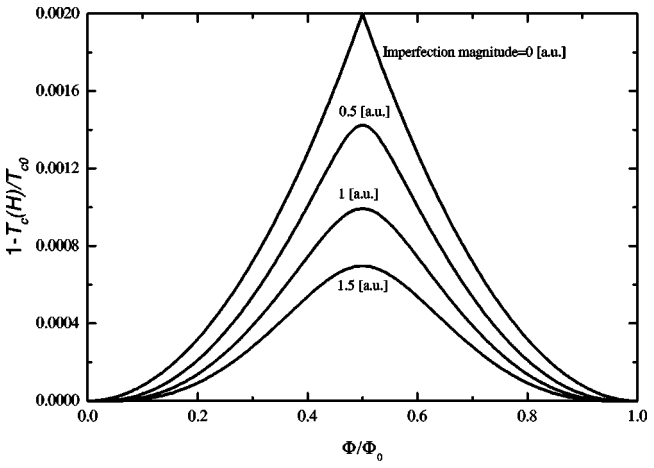

FIG. 5. The calculated phase boundary is shown for one period using the micronet approach for a loop containing one scattering imperfection (Ref. 13). The different curves correspond to different magnitudes of the scattering imperfection: from zero magnitude for the upper curve to a large magnitude for the lowest curve.

related to the presence of scattering imperfections in the outer loop of sample A, as has been shown theoretically in Ref. 13. A possible source of such imperfections could be the variation of the strip width along the loops written by e-beam lithography. Using the micronet approach,[14,15] the GL equation can also be solved when imperfections are present in a loop. A single period of the phase boundary calculated from this micronet approach[13] is presented in Fig. 5 for different magnitudes of imperfections. Notice that the stronger the imperfection the more the oscillation amplitude is damped.

It is clear from our experiments and from Ref. 9 that the influence of the inner loop on the measured phase boundary is quite small. To detect traces of the periodicity coming from the $T_c(\Phi)$ oscillations of the inner loop, a fast Fourier transform analysis of the phase boundaries is carried out using 2^{10} equally spaced points in an interval between 5 and 24 Φ/Φ_0 for sample A, B, and R and between -36 and 49 Φ/Φ_0 for sample C, but with approximately the same number of data points. In order to remove most of the contribution arising from the fluxoid quantization in the outer loop, the parabolas fitted in Figs. 3, 4(a), and 4(b) (solid line) are subtracted from the experimental data, prior to taking the Fourier transform. The resulting spectra are presented in Figs. 6(a) for sample A, 6(b) for sample B, 6(c) for sample C, and 6(d) for the single loop (sample R), for an external transport current of $I_t=0.3$ μA. The Fourier spectra of sample A and sample R for $I_t=0.5$ μA are shown in Figs. 7(a) and 7(b), respectively.

In Figs. 6(a), 6(c), and 7(a), a peak is clearly seen at $(\Phi/\Phi_0)^{-1}=1$ corresponding to the frequency of the LP oscillations for the outer loop; the second to the sixth harmonics of this base frequency are also seen. In the case of the sample R [Figs. 6(d) and 7(b)] and of sample B [Fig. 6(b)], the first harmonic is strongly reduced. This reduction is quite reasonable because of the subtraction procedure applied before the Fourier transformation. The lower scale for the Fourier spectrum for sample C [Fig. 6(c)] is probably due to a smaller amplitude of the oscillations in the phase boundary. For the double loop (samples A, B, and C), supplementary peaks are clearly distinguished in between the harmonics [see inset in Figs. 6(a), 6(b), 6(c), and 7(a)], which are considerably weaker in the reference sample R. These peaks can be due to the coupling with the supercurrent in the inner loop. Comparing the insets of Fig. 6(b) and Fig. 6(d), we note that the supplementary peaks are substantially sharper and higher for sample B than for sample R.

The period of the LP oscillations for the outer loop is $\mu_0\Delta H_o=\Phi_0/S_o=0.525$ mT and $\mu_0\Delta H_o=0.550$ mT for samples A, B, and R and for sample C, respectively, corresponding to the first harmonic peak at $(\Phi/\Phi_0)^{-1}=1$. The periodicity of the $T_c(\Phi)$ oscillations for the inner loop (samples A and B) is $\mu_0\Delta H_i=\Phi_0/S_i=2.6$ mT, which is approximately 5 times larger than $\mu_0\Delta H_o$, since the surface of the inner loop is approximately 5 times smaller than the one of the outer loop. This periodicity is in good agreement with the measurement on sample B [Fig. 6(b)], where four peaks are indeed observed between the first and the second harmonic, thus indicating a five times smaller frequency compared to the frequency of the $T_c(\Phi)$ oscillations of the outer loop. The $T_c(\Phi)$ measurements on sample A show two pronounced peaks between each harmonic [Figs. 6(a) and 7(a)]. This suggests a period for the inner loop $\mu_0\Delta H_i \approx 3\mu_0\Delta H_o$ which is in disagreement with the dimensions of sample A. For sample C, which has a slightly different size, the periodicity of the inner loop oscillations in $T_c(\Phi)$ is $\mu_0\Delta H_i=\Phi_0/S_i=2.1$ mT$\approx 4\mu_0\Delta H_o$. This periodicity is in agreement with the measurements where three peaks are clearly observed before the first harmonic [see Fig. 6(c)].

The reason for the disagreement between the periodicity of the oscillations and the peaks in the Fourier spectrum of sample A can be a different effective surface. To calculate the periodicity of the oscillations of the inner and outer loop, the average size of the loops (through the middle of the wires) has been used. It is possible that we have to take a slightly smaller or larger effective surface for sample A. The dimensions of samples A and B may also be not exactly the same. But the effective surface has to be taken larger than the largest dimensions of the inner loop to obtain a value of $\mu_0\Delta H_i \approx 3\mu_0\Delta H_o$. We therefore think that the smaller peaks might be hidden, and not clearly seen however in the Fourier spectrum. In that case, a value for the periodicity of 6 times the periodicity of the inner loop is more realistic for sample A. Coming back to Fig. 2, we can see that the interval (between 5 and 24 Φ/Φ_0), where a Fourier transform was performed for samples A, B, and R, corresponds only to 3 or 4 periods $\mu_0\Delta H_i$. The resolution of the Fourier spectrum in the low frequency regime will therefore be low, thus presenting an additional difficulty in interpreting the intermediate peaks in the Fourier spectra. The phase boundary $T_c(\Phi)$ of sample C is measured over a broader interval (between -36 to 49 Φ/Φ_0). This interval corresponds to more than 20 periods $\mu_0\Delta H_i$, which results in a better resolution of the Fourier spectrum in the low frequency regime.

In a first approximation, with the currents I_i and I_o independent from each other, the mutual inductance M can be evaluated from the amplitude of the additional peaks in the Fourier spectrum. The additional energy due to the mutual

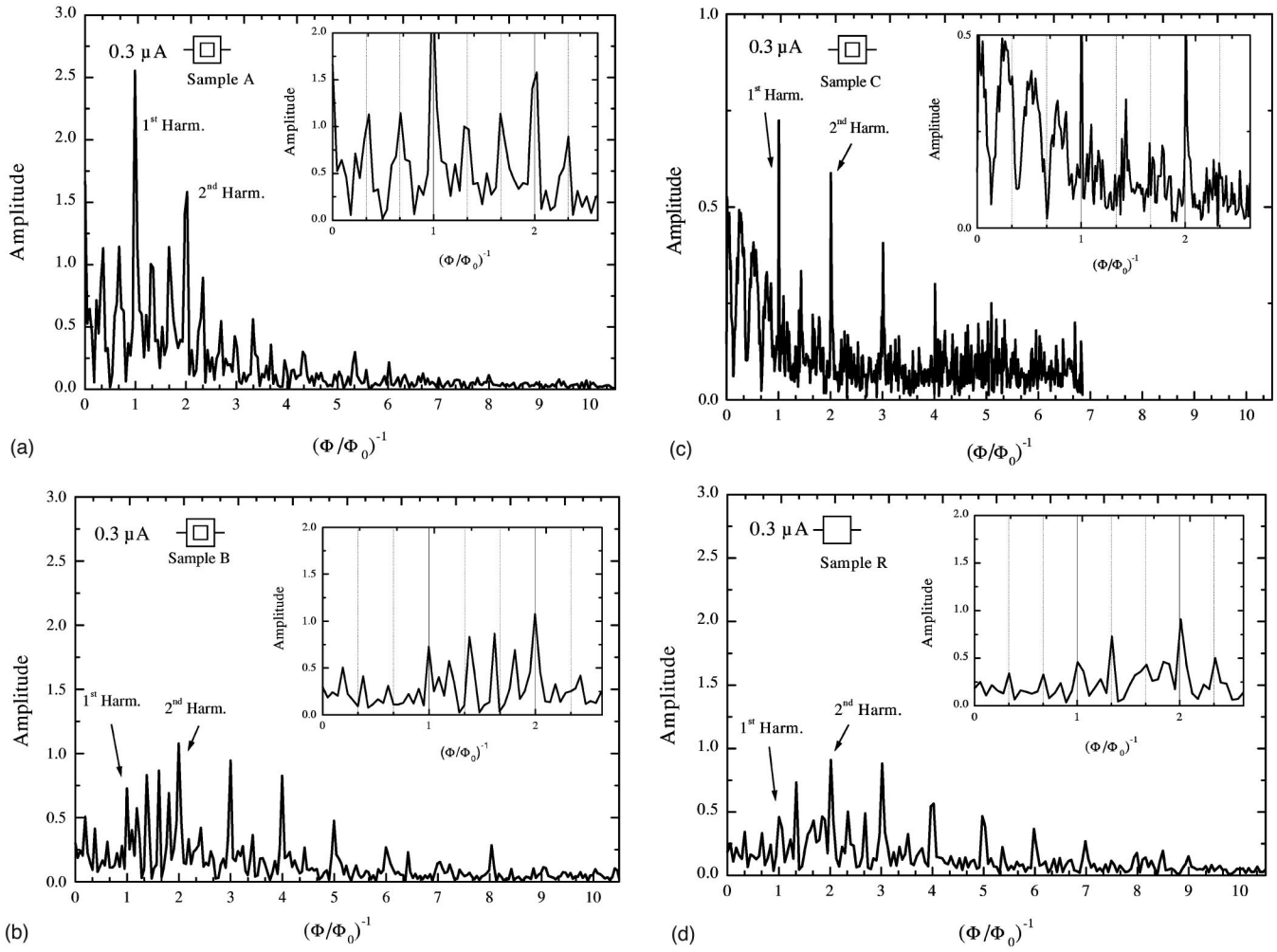

FIG. 6. Fourier transform of the phase boundary after subtraction of the fitted parabolas within each oscillation period, for a transport current $I_t = 0.3\ \mu$A for (a) sample A, (b) sample B, (c) sample C, and (d) sample R. The inset shows a zoom of the plot for the low frequency region.

inductance in Eq. (4) (MI_iI_o) has to be of the same order of magnitude as the amplitude of the oscillations $k_B\Delta T_{\text{coupling}}$ due to coupling in the phase boundary of the outer loop. The value for the mutual inductance can then be evaluated with the formula

$$M \approx \frac{k_B \Delta T_{\text{coupling}}}{\langle I_i I_o \rangle}, \tag{7}$$

with k_B the Boltzmann constant. This gives $M \approx 17$ pH, 13 pH, and 14 pH for samples A, B, and C, respectively. The average of the supercurrents I_i and I_0 is calculated from Refs. 7 and 9, for $I_t = 0.3\ \mu$A and with the criterion for T_{co} at 90% of R_n, which correspond to a typical temperature interval of 3 mK between this criterion and the 50% criterion used for the measurements of the phase boundary. It is quite clear that the supercurrents, and thus also the mutual inductance are strongly dependent of this chosen criterion. The values calculated from Eq. (7) are comparable to the calculated mutual inductances from Table I. Due to the strong temperature dependent currents, only the order of magnitude of the mutual inductance can be evaluated from our measurements.

For high ($I_t = 0.9\ \mu$A for sample A and 1.0 μA for sample C) transport current, the peaks between the harmonics completely disappear (not shown). This vanishing may be due to increasing shift of $T_c(\Phi)$ with the applied transport current. The highest current corresponds to the case of the upper curve (dashed-dotted line) in Fig. 2. Hence, for all flux values, the inner loop is in the superconducting state at $T_c(\Phi)$ of the outer loop, and the phase boundaries of the two loops are not intersecting each other. There will be no sharp interruption of the supercurrent of the inner loop going from the superconducting to the normal state. Therefore, the shape of the phase boundary of the outer loop can be less sensitive to the presence of the inner loop. On the other hand, once the inner loop is deep in the superconducting state, a higher supercurrent in the inner loop would be present, and this higher supercurrent would require a higher coupling. If the transport current I_t is high enough, the inner loop will be always su-

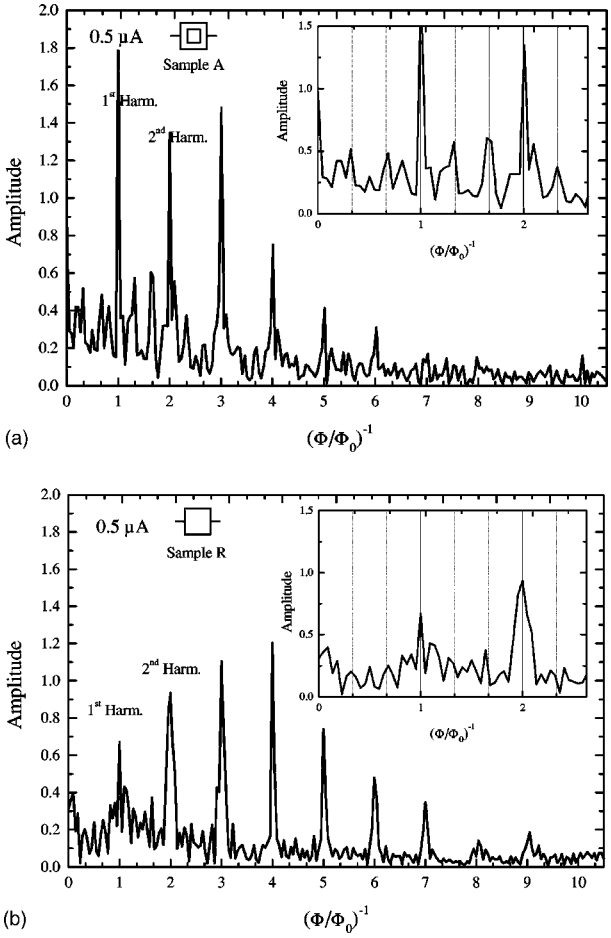

FIG. 7. Fourier transform of the phase boundary after subtraction of the fitted parabolas within each oscillation period, for a transport current $I_t = 0.5\ \mu$A for (a) sample A and (b) sample R. The inset shows a zoom of the plot for the low frequency region.

perconducting at $T_c(\Phi)$ of the outer loop. A discontinuity in the measured phase boundary of the outer loop is expected when the inner loop changes from a fluxoid quantum number N_i to $N_i \pm 1$. However, we could not see a discontinuity in the measured phase boundaries, corresponding to a sign reversal of the supercurrent in the inner loop.

III. CONCLUSION

We have measured the normal/superconducting phase boundary of a superconducting system consisting of two concentric mesoscopic loops, to study magnetic interactions between the two loops. The modification of the $T_c(\Phi)$ oscillations of the outer loop is seen in the Fourier spectrum of the $T_c(\Phi)$ line due to the coupling between the outer and the inner loops. To interpret these observations, we have used two different models. The first model assumes the presence of scattering imperfections in the outer loop. This model cannot explain the observed evolution of the Fourier spectrum with the current, although it might be applicable for a fixed weak current. The second model explains the extra peaks in the Fourier spectrum by the magnetic coupling of the two loops. The systematic shift of the $T_c(\Phi)$ phase boundary of the outer loop with the applied current I_t induces a well defined evolution of the Fourier spectrum which was indeed found in our experiments. This evolution of the extra peaks in the Fourier spectrum with the applied current gives an experimental evidence for the presence of the magnetic interaction between the two superconducting loops.

Future magnetic measurements on huge arrays of magnetically coupled loops, deeper in the superconducting state, could be helpful to reveal an enhanced magnetic coupling of both loops at lower temperatures. An inner loop made from a different superconductor with a higher critical temperature would certainly increase the magnetic coupling between the two loops. An enhanced critical field is expected in this case for the lower T_c loop, at the expense of sharing the fluxoid quantization ''burden'' with a loop where superconductivity is stronger.

ACKNOWLEDGMENTS

The authors wish to thank M. Cannaerts, E. Seynaeve, and K. Temst for the AFM, SEM, and x-ray measurements, and H.J. Fink and L. Van Look for useful discussions. This work has been supported by the Belgian IUAP, the FWO and GOA programs, and by the ESF Program VORTEX.

[1] W.A. Little and R.D. Parks, Phys. Rev. Lett. **9**, 9 (1962); R.D. Parks and W.A. Little, Phys. Rev. **133**, A97 (1964).
[2] F. London, *Superfluids* (Wiley, New York, 1950).
[3] M. Tinkham, *Introduction to Superconductivity* (McGraw-Hill, New York, 1975).
[4] P.-G. de Gennes, *Superconductivity of Metals and Alloys* (Benjamin, New York, 1966).
[5] J.X. Zhu, Z.D. Wang, and Q. Wang, J. Phys. Soc. Jpn. **65**, 2602 (1996).
[6] J. Wang, and Z.S. Ma, Phys. Rev. B **52**, 14 829 (1995).
[7] D. Davidovic, S. Kummar, D.H. Reich, J. Siegel, S.B. Field, R.C. Tiberio, R. Hey, and K. Ploog, Phys. Rev. Lett. **76**, 815 (1996); Phys. Rev. B **55**, 6518 (1997).
[8] M. Tinkham, Phys. Rev. **129**, 2413 (1963).
[9] X. Zhang and J.C. Price, Phys. Rev. B **55**, 3128 (1996).
[10] C. Strunk, V. Bruyndoncx, C. Van Haesendonck, V.V. Moshchalkov, and Y. Bruynseraede, Phys. Rev. B **53**, 11 332 (1996).
[11] J. Romijn, T.M. Klapwijk, M.J. Renne, and J.E. Mooij, Phys. Rev. B **26**, 3648 (1982).
[12] W. J. Duffin, *Electricity and Magnetism* (McGraw-Hill, London, 1998); J. D. Jackson, *Classical Electrodynamics* (Wiley, New York, 1999).
[13] V.M. Fomin, J.T. Devreese, V. Bruyndoncx, and V.V. Moshchalkov, Phys. Rev. B **62**, 9186 (2000).
[14] H.J. Fink, A. López, and R. Maynard, Phys. Rev. B **26**, 5237 (1982).
[15] S. Alexander, Phys. Rev. B **27**, 1541 (1983).